

# Co-doped Ni(OH)<sub>2</sub> Ultrafine Particles with High Supercapacitor Performance

Qiannan Feng<sup>1</sup>, Feng Liu<sup>1</sup>, Jiongliang Yuan<sup>1,\*</sup>, Qinghong Xu<sup>2,\*</sup>

<sup>1</sup> Department of Environmental Science and Engineering, Beijing University of Chemical Technology, Beijing 100029, P.R. China

<sup>2</sup> State Key Laboratory of Chemical Resource Engineering, Beijing University of Chemical Technology, Beijing 100029, P.R. China

\*E-mail: [yuanjiongliang@163.com](mailto:yuanjiongliang@163.com) (Jiongliang Yuan), [xuqh@mail.buct.edu.cn](mailto:xuqh@mail.buct.edu.cn) (Qinghong Xu)

Received: 2 September 2019 / Accepted: 18 October 2019 / Published: 10 March 2020

Ni(OH)<sub>2</sub> and Co-doped Ni(OH)<sub>2</sub> ultrafine particles were synthesized by coprecipitation method. When the molar ratio of Ni<sup>2+</sup>:Co<sup>2+</sup> in the precursor solution was 5:1, the resulted Co-doped Ni(OH)<sub>2</sub> ultrafine particles displayed a high specific capacitance of 669.57 F g<sup>-1</sup> at a current density of 1 A g<sup>-1</sup>, and 94% initial specific capacitance remained after 500 charge-discharge cycles at a current density of 16 A g<sup>-1</sup>, showing better electrochemical performance than Ni(OH)<sub>2</sub> ultrafine particles. The introduction of Co<sup>2+</sup> improved the electrochemical performance of Ni(OH)<sub>2</sub> electrode material.

**Keywords:** Co-doped Ni(OH)<sub>2</sub>, ultrafine particles, coprecipitation, supercapacitor.

## 1. INTRODUCTION

With rapid development of the global economy, the consumption of fossil fuels (oil, coal, etc.) is increasing at an alarming rate. Energy shortage and environmental pollution have become two major obstacles to human development. Therefore, it is urgent to develop new energy sources that are efficient, clean and sustainable. Meanwhile, the development of advanced energy conversion and storage technologies plays an important role in maintaining the balanced development of the global economy [1-3]. Among various energy storage systems, electrochemical energy storage technologies, such as lithium ion batteries, fuel cells, and supercapacitors, are the most widely used. As a new type of environmentally-friendly and high-efficiency energy storage device, supercapacitor has higher energy density than conventional capacitors and higher power density than secondary batteries (lithium batteries). At the same time, it has many advantages such as long cycle life, high charge-discharge efficiency, wide operating temperature range, etc. Therefore it has attracted extensive attention in the

field of energy storage [4]. In recent years, supercapacitors are mainly used in some portable electronic products, mobile devices and energy recovery systems generated during braking. In the future, supercapacitor technology will also have the same important status as lithium battery in the field of new energy transportation.

In general, supercapacitors can be classified into two types according to their energy storage mechanisms: electric double layer capacitors and pseudocapacitors [5]. The electric double layers depend on electric double layer generated by charge separation at the electrode/electrolyte interface to store energy. Carbon materials (activated carbon, graphene, carbon nanotubes, etc.) having a high specific surface area and high electrical conductivity are often used as electrode materials for electric double layer capacitors. Pseudocapacitors depend on a fast reversible redox reaction on the surface (or subsurface) of the electrode to store energy. Metal oxides/hydroxides, metal sulfides, and conductive polymers that follow the pseudocapacitor mechanism have been widely studied as pseudocapacitor electrode materials [6]. Ni(OH)<sub>2</sub> has received special attention due to its high specific capacitance, low cost and good electrochemical redox activity. However, Ni(OH)<sub>2</sub> is a p-type semiconductor with poor electronic conductivity, which limits its application. In order to improve its electrochemical performance, Ni(OH)<sub>2</sub> needs to be doped and/or surface modified. In recent years, the preparation of double hydroxide electrode materials has received intensive attention. Double hydroxide can exert the synergistic effect of various materials, increase the specific surface area, promote electron transfer, and improve the cycling stability [7,8]. A large number of studies have shown that the doping of Co<sup>2+</sup> can effectively improve electrochemical performance of Ni(OH)<sub>2</sub> [9-12]. Xu et al. [13] synthesized a urchin-like Ni(OH)<sub>2</sub>-Co(OH)<sub>2</sub> hollow microsphere by microwave-incorporated hydrothermal method. The Ni(OH)<sub>2</sub>-Co(OH)<sub>2</sub> hollow microspheres have a high specific capacitance of 2164 F g<sup>-1</sup> at 1 A g<sup>-1</sup> and long cycle life compared to Ni(OH)<sub>2</sub> (1807 F g<sup>-1</sup>) and Co(OH)<sub>2</sub> (551 F g<sup>-1</sup>) at the same current density. Liu et al. [14] successfully grew Co-doped α-Ni(OH)<sub>2</sub> multi-dimensional structure on nickel foam. This Co-doped α-Ni(OH)<sub>2</sub> material exhibited a specific capacitance of 2897.76 F g<sup>-1</sup> at the current density of 1 A g<sup>-1</sup>. And after 3000 charge-discharge cycles, the coulomb efficiency is as high as 98.8%, showing excellent electrochemical performance.

In this paper, Ni(OH)<sub>2</sub> and Co-doped Ni(OH)<sub>2</sub> ultrafine particles were synthesized by coprecipitation method. The doping of Co<sup>2+</sup> plays an important role in increasing the electrical performance of Ni(OH)<sub>2</sub>.

## 2. EXPERIMENTAL

### 2.1 Chemicals

In the experiment, NaOH, glucose, Ni(NO<sub>3</sub>)<sub>2</sub>·6H<sub>2</sub>O and CoCl<sub>2</sub>·6H<sub>2</sub>O were purchased from Beijing Chemical Reagent Company (Beijing, PR China). The chemicals used in this experiment were analytical grade and used without further purification. Deionized water was used through the experiment.

## 2.2 Synthesized of electrode materials

0.1 g of NaOH and 20 g of glucose were added to 100 mL of deionized water, stirred and fully dissolved.  $5 \times 10^{-5}$  mol of  $\text{CoCl}_2 \cdot 6\text{H}_2\text{O}$  was added to 100 mL of  $0.01 \text{ mol L}^{-1}$   $\text{Ni}(\text{NO}_3)_2$  solution. The mixed solution was added dropwise to the prepared glucose alkaline solution at a dropping rate of about  $1 \text{ drop s}^{-1}$ . After completion of the dropwise addition, the mixture was quickly transferred to a high-speed centrifugal machine and centrifuged at 8000 rpm for 10 min. The resulted precipitate was washed 10 times with deionized water and then dried overnight. Thus Co-doped  $\text{Ni}(\text{OH})_2$  ultrafine particles with Ni:Co molar ratio of 20:1 was obtained, which was denoted as 1Co-Ni(OH)<sub>2</sub>. Co-doped  $\text{Ni}(\text{OH})_2$  ultrafine particles with Ni:Co molar ratio of 10:1 and 5:1 were denoted as 2Co-Ni(OH)<sub>2</sub> and 3Co-Ni(OH)<sub>2</sub>. The synthesis of  $\text{Ni}(\text{OH})_2$  ultrafine particles is referred to reference 15.

## 2.3 Material Characterization

The morphology of the synthesized ultrafine particles was observed using an S-4700 field emission scanning electron microscope (SEM, Hitachi, Japan). The crystal structure of the samples were investigated by X-ray diffraction analyzer (XRD, Bruker D8 Advance, Germany) with Cu K $\alpha$  radiation ( $\lambda=0.154\text{nm}$ ). The x-ray photoelectron spectra (XPS) were measured by ESCALAB 250 (ThermoFisher Scientific, USA) equipped with x-ray source of twin anode Al K $\alpha$  300W. The XPS spectrometer was configured to operate with 200 eV pass energy for survey, and 30 eV for high resolution scans. All binding energies were calibrated to C1s at 284.6 eV. The chemical compositions of the samples were analyzed by energy dispersive X-ray spectroscopy (EDS, JEOL, Japan).

## 2.4 Preparation of the electrodes

The nickel foam substrate (1×3 cm) was ultrasonically washed in  $1 \text{ mol L}^{-1}$  of dilute hydrochloric acid, acetone, ethanol and deionized water for 10 min, respectively, and finally dried in a vacuum oven for 24 h.

Typically, 80wt.% ultrafine powder, 10wt.% acetylene black as a conductive agent, 10wt.% polytetrafluoroethylene (PTFE) as a binder, were uniformly mixed. The formed slurry was uniformly coated on the treated nickel foam substrate with a coating area of about  $1 \text{ cm}^2$ , and the prepared electrode was dried in a vacuum oven for 24 h.

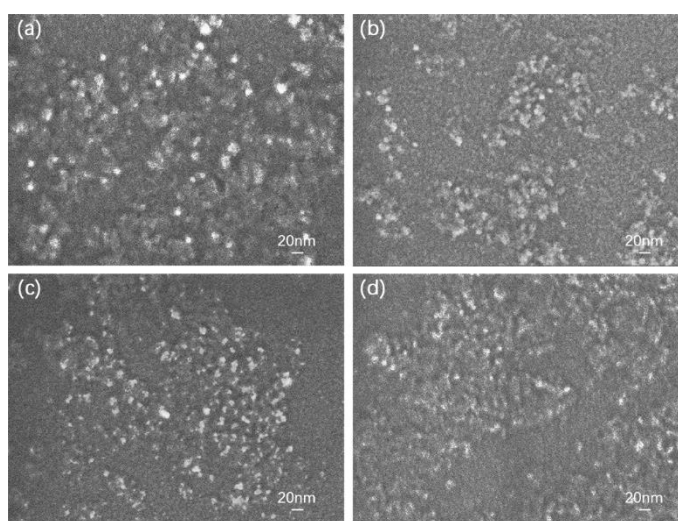
## 2.5 Electrochemical measurement

Electrochemical testing was performed on a CHI660E electrochemical workstation (Shanghai CH Instrument Company, PR China) at room temperature ( $25 \text{ }^\circ\text{C}$ ). All tests were performed using a three-electrode system in an aqueous 6.0 M KOH solution. Co-Ni(OH)<sub>2</sub> electrode, platinum mesh (1.5 ×1.5 cm) and Hg/HgO electrode (1.0 M KOH as salt bridge solution) were used as the working electrode, counter electrode and reference electrode, respectively.

The cyclic voltammetry curves (CV) of the electrodes were tested in range of 0 to 0.5 V at various scan rates (50, 20, 10, 5 and 2  $\text{mV s}^{-1}$ ). Galvanostatic charge-discharge testing was performed at various current density (1, 2, 4, 8 and 16  $\text{A g}^{-1}$ ) in range of 0 to 0.5 V. 500 galvanostatic charge-discharge cycles were performed at 16  $\text{A g}^{-1}$  to evaluate cycle stability of the electrodes. The electrochemical impedance spectroscopy (EIS) was tested in range of 10 mHz to 100 kHz with an amplitude of 5 mV.

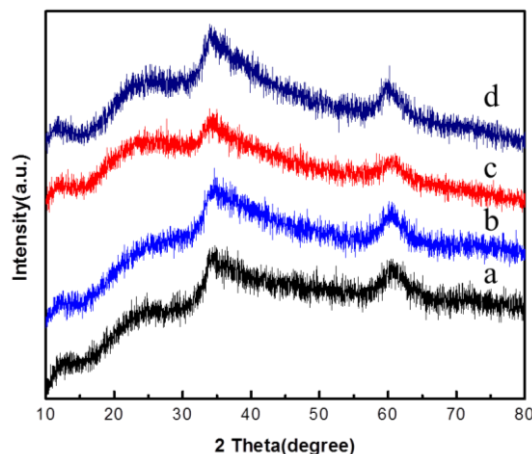
### 3. RESULTS AND DISCUSSION

#### 3.1 Microstructure



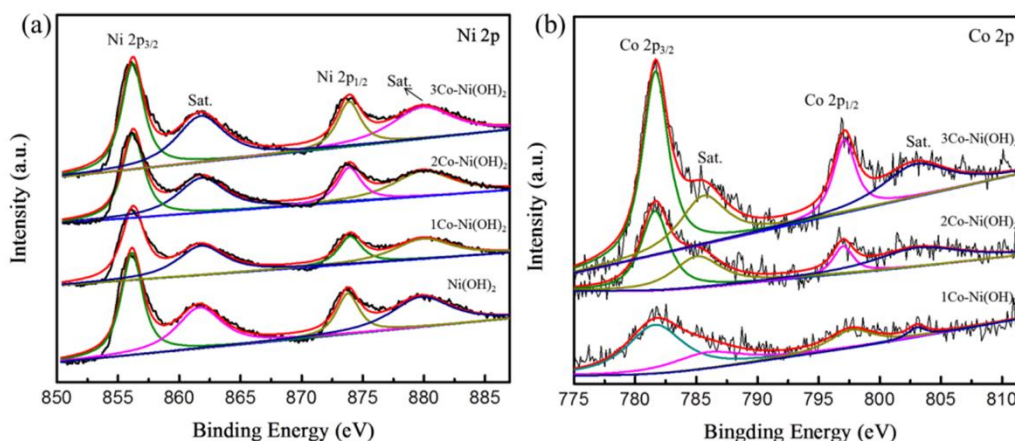
**Figure 1.** SEM images of  $\text{Ni(OH)}_2$  (a),  $1\text{Co-Ni(OH)}_2$  (b),  $2\text{Co-Ni(OH)}_2$  (c) and  $3\text{Co-Ni(OH)}_2$  (d) ultrafine particles

Fig.1 exhibits the SEM images of  $\text{Ni(OH)}_2$ ,  $1\text{Co-Ni(OH)}_2$ ,  $2\text{Co-Ni(OH)}_2$  and  $3\text{Co-Ni(OH)}_2$  ultrafine particles synthesized by coprecipitation method. As can be seen from the figure, all the samples show ultrafine spherical particles with a particle size distribution of about 5-15 nm. Due to hydrogen bonds between glucose and water molecules, "some confined spaces" were formed in the glucose alkaline solution, which limit the combination of metal ions and  $\text{OH}^-$  ions in a small space, therefore ultrafine particles were obtained [15]. The morphologies of ultrafine particles were not affected by the additional  $\text{Co}^{2+}$  ions.



**Figure 2.** XRD patterns of Ni(OH)<sub>2</sub> (a), 1Co-Ni(OH)<sub>2</sub> (b), 2Co-Ni(OH)<sub>2</sub> (c) and 3Co-Ni(OH)<sub>2</sub> (d) ultrafine particles

XRD patterns of all samples are showed in Fig.2. The diffraction peaks at  $2\theta$  values of  $12.1^\circ$ ,  $24.6^\circ$ ,  $33.3^\circ$  and  $59.9^\circ$  are indexed to Ni(OH)<sub>2</sub> (003), (006), (101) and (110) planes (JCPDS Card No.38-0715), respectively. The XRD patterns of Co-doped Ni(OH)<sub>2</sub> materials are similar to that of pure Ni(OH)<sub>2</sub> and phases of the doped Co ion were not detected, this is because the positions of Ni<sup>2+</sup> are occupied by Co<sup>2+</sup>. The similar radius of Co<sup>2+</sup> and Ni<sup>2+</sup> results in little changes in their crystal structures and peak positions, so it is not easy to observe. It is indicated that the Co-doped Ni(OH)<sub>2</sub> composites have been well synthesized [10].



**Figure 3.** XPS spectra of Ni 2p for all samples (a) and Co 2p for Co-Ni(OH)<sub>2</sub> samples (b)

XPS spectra of Ni 2p and Co 2p in the samples are shown in Fig.3. The two peaks at 855.9 and 873.5 eV correspond to Ni 2p<sub>3/2</sub> and Ni 2p<sub>1/2</sub> in all the samples, respectively, with the spin-energy separation of 17.6 eV, which are characteristic of a Ni(OH)<sub>2</sub> phase [16,17]. Moreover, the satellite peaks located at 861.8 and 880.2 eV are observed [18]. The peaks at 781.1 and 796.2 eV in Fig. 3 (b)

correspond to Co 2p<sub>3/2</sub> and Co 2p<sub>1/2</sub> in Co(OH)<sub>2</sub>, respectively. In addition, two shakeup satellites at 786.5 and 802.9 eV further confirm the existence of Co(OH)<sub>2</sub> [19].

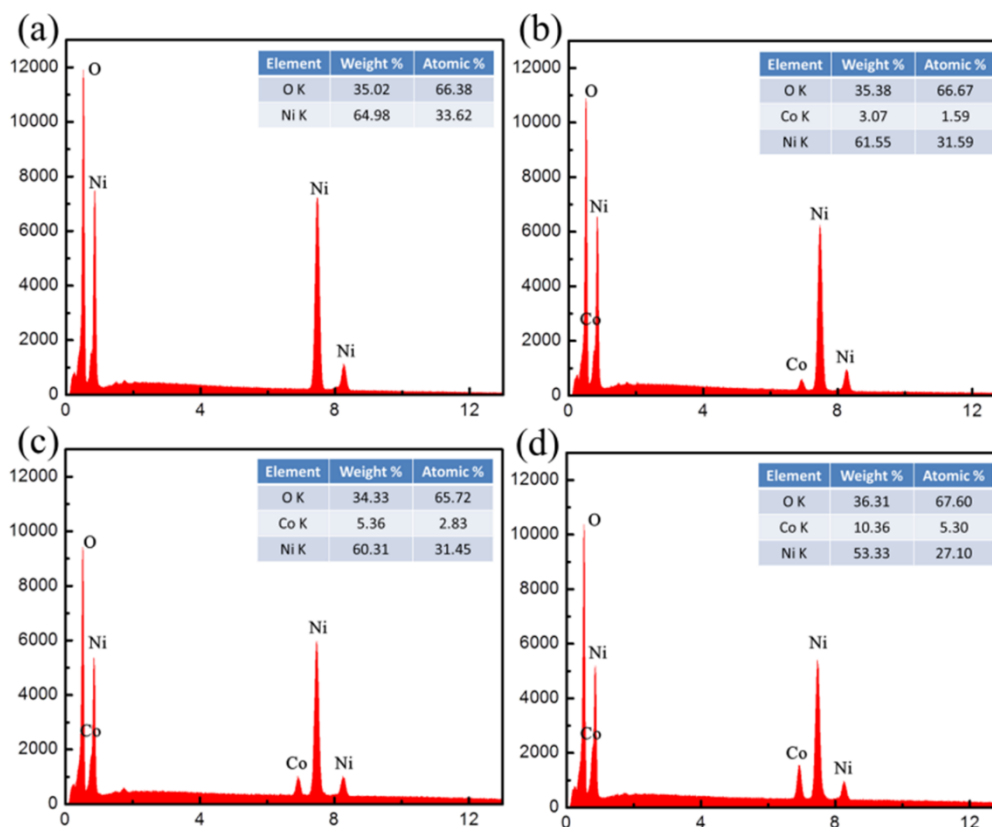


**Figure 4.** EDS results of Ni(OH)<sub>2</sub> (a), 1Co-Ni(OH)<sub>2</sub> (b), 2Co-Ni(OH)<sub>2</sub> (c) and 3Co-Ni(OH)<sub>2</sub> (d)

**Table 1.** Chemical composition of Ni(OH)<sub>2</sub> and Co-Ni(OH)<sub>2</sub> samples

Sample	Ni/Co (mol/mol)	O/(Ni+Co)(mol/mol)
Ni(OH) <sub>2</sub>	—	1.98
1Co-Ni(OH) <sub>2</sub>	19.87	2.01
2Co-Ni(OH) <sub>2</sub>	11.11	1.92
3Co-Ni(OH) <sub>2</sub>	5.11	2.09

The chemical composition of each electrode material is determined by EDS analysis (shown in Fig.4), and the atomic ratio of Ni/Co and O/(Ni+Co) are calculated (listed in Table 1). The results show that the atomic ratio of O/Ni in Ni(OH)<sub>2</sub> electrode material is 1.98, closing to the stoichiometric ratio of Ni<sup>2+</sup> and OH<sup>-</sup> in Ni(OH)<sub>2</sub>. In addition, the molar ratio of Ni/Co is closed to 20, 10, 5 in 1Co-Ni(OH)<sub>2</sub>, 2Co-Ni(OH)<sub>2</sub>, 3Co-Ni(OH)<sub>2</sub> sample, respectively, indicating that the Ni/Co molar ratio in the precursor solution is maintained.

3.2 Electrochemical properties

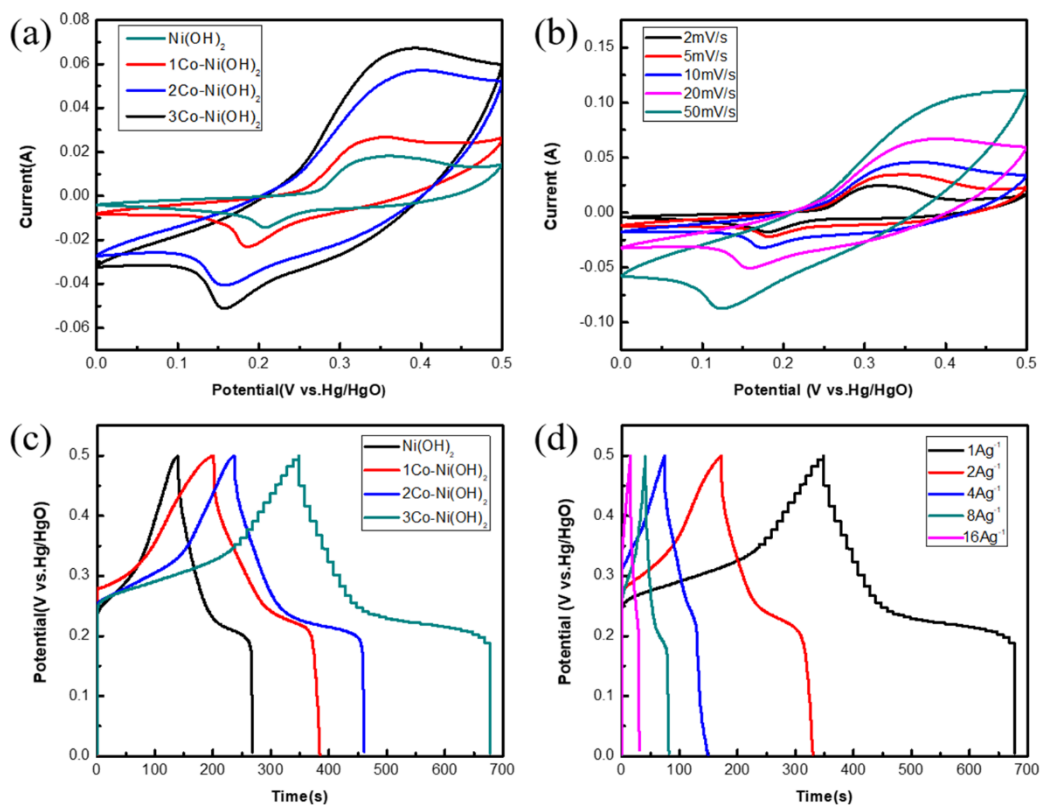


**Figure 5.** (a) CV curves of Ni(OH)<sub>2</sub>, 1Co-Ni(OH)<sub>2</sub>, 2Co-Ni(OH)<sub>2</sub>, 3Co-Ni(OH)<sub>2</sub> electrodes at a scan rate of 20 mV s<sup>-1</sup>; (b) CV curves of 3Co-Ni(OH)<sub>2</sub> electrode at scan rate from 2 to 50 mV s<sup>-1</sup>; (c) GCD curves of Ni(OH)<sub>2</sub>, 1Co-Ni(OH)<sub>2</sub>, 2Co-Ni(OH)<sub>2</sub>, 3Co-Ni(OH)<sub>2</sub> electrodes at a current density of 1 A g<sup>-1</sup>; (d) GCD curves of 3Co-Ni(OH)<sub>2</sub> at current density from 1 to 16 A g<sup>-1</sup>.

The CV curves of the electrodes (shown in Fig.5) are tested at a scan rate of 20 mV s<sup>-1</sup> in the potential range from 0 to 0.5 V. A couple of redox peaks can be observed in each CV curve, indicating that their electrochemical capacitance is mainly derived from Faraday reaction and pseudocapacitance [13]. The redox reaction of Ni(OH)<sub>2</sub> electrode can be expressed by the following equation [20]:



In the CV curve of Ni(OH)<sub>2</sub> electrode, the anode peak corresponds to oxidation of Ni(OH)<sub>2</sub> to NiOOH, and the cathode peak corresponds to reverse process [21]. It can be seen that the CV integral area of 3Co-Ni(OH)<sub>2</sub> electrode is larger than those of other electrodes. Fig.5 (b) is CV curves of the 3Co-Ni(OH)<sub>2</sub> electrode at a scan rate of 2, 5, 10, 20, 50 mV s<sup>-1</sup>, respectively. The peak current increases with increase of the scan rate; however, the shape of the curve remains unchanged, showing excellent rate performance. In addition, the oxidation peak shifts positively and the reduction peak shifts negatively as scan rate increases, which is caused by an increase in internal diffusion resistance [14].

In order to investigate discharge specific capacitance values of the electrodes, the galvanostatic charge-discharge (GCD) experiments were carried out. In potential range from 0 to 0.5 V, the

galvanostatic charge-discharge behavior of each electrode in a 6 mol L<sup>-1</sup> KOH electrolyte at a current density of 1 A g<sup>-1</sup> is shown in Fig.5 (c). All galvanostatic charge and discharge curves of Ni(OH)<sub>2</sub> and Co-Ni(OH)<sub>2</sub> electrodes exhibit pseudocapacitance characteristics, which are consistent with the results of CV test. In GCD curve, the vertical variation portion corresponds to charge separation at the electrode/electrolyte interface, and oblique variation portion corresponds to the electrochemical redox reaction [22]. In addition, it can be observed from the figure that the discharge time of 3Co-Ni(OH)<sub>2</sub> electrode is highest among all the electrodes. The discharge specific capacitance of the electrode during galvanostatic charge-discharge can be calculated by the following equation [23]:

$$C_{sp} = \frac{I\Delta t}{m\Delta V} \quad (2)$$

Where  $C_{sp}$  (F g<sup>-1</sup>) is the discharge specific capacitance,  $m$  (g) is the mass of the active material,  $\Delta V$  (V) is the potential range,  $I$  (A) is the applied discharge current, and  $\Delta t$  (s) is the discharge time.

The specific capacitance of 1Co-Ni(OH)<sub>2</sub>, 2Co-Ni(OH)<sub>2</sub>, and 3Co-Ni(OH)<sub>2</sub> electrode reaches 367.42, 450.42 and 669.57 F g<sup>-1</sup> at a current density of 1 A g<sup>-1</sup>, respectively, higher than that of Ni(OH)<sub>2</sub> electrode (259.56 F g<sup>-1</sup>). In order to further investigate the electrochemical properties of 3Co-Ni(OH)<sub>2</sub> electrode, GCD curves of the electrode were tested at various current density, which are showed in Fig.5 (d). Obviously, the discharge time gradually decreases as the current density increases, similar to previous studies [18,24,25]. As current density increases, the transfer rate of electron/ion increases. As a result, the effective interaction between the electron/ion and the electrode is reduced, leading to a reduction in discharge time. The specific capacitance of 3Co-Ni(OH)<sub>2</sub> electrode is 602.39, 568.71, 481.25 and 384.11 F g<sup>-1</sup> at 2, 4, 8 and 16 A g<sup>-1</sup>, corresponding to 90, 85, 72 and 57% of the specific capacitance values at 1 A g<sup>-1</sup>, respectively. When current density increases sequentially, the specific capacitance fading is smaller than those of Ni(OH)<sub>2</sub> electrode (89, 80, 69 and 61%, respectively), indicating that redox reaction can occur quickly in 3Co-Ni(OH)<sub>2</sub> electrode at high current density. The formation of conductive CoOOH in ultrafine particles during the charge process accounts for the specific capacitance increase and slow attenuation of 3Co-Ni(OH)<sub>2</sub> electrode. CoOOH can effectively improve the conductivity of Ni(OH)<sub>2</sub> electrode, which results in higher active material utilization rate and faster charge transfer [26]. The polarization participation increases with the increase of current density, which explains why the value of specific capacitance decreases with the increase of current density [27].

Cycle stability is very vital for assessing the practical application of energy storage materials. The cyclic stability of the Ni(OH)<sub>2</sub> and 3Co-Ni(OH)<sub>2</sub> materials was examined by a galvanostatic charge-discharge experiment for 500 cycles at a high current density of 16 A g<sup>-1</sup>, as shown in Fig.6. It is clear that the 3Co-Ni(OH)<sub>2</sub> electrode retains 94% of the initial specific capacitance after 500 cycles, showing high cycle stability. The results suggest that the 3Co-Ni(OH)<sub>2</sub> material has long-term electrochemical stability and high charge-discharge reversibility.

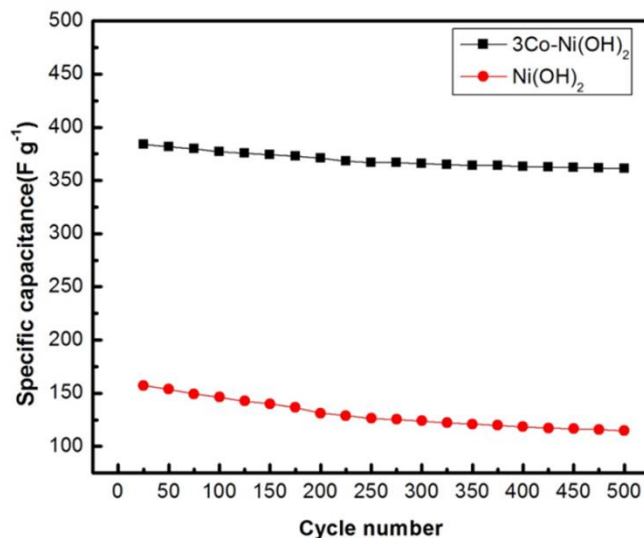


**Figure 6.** Cycling performance of Ni(OH)<sub>2</sub> and 3Co-Ni(OH)<sub>2</sub> materials in a 6 M KOH electrolyte measured using the galvanostatic charge-discharge technique at a current density of 16 A g<sup>-1</sup>.

The electrochemical performances of 3Co-Ni(OH)<sub>2</sub> and other materials in literatures are compared in Table 2. It can be seen that the 3Co-Ni(OH)<sub>2</sub> shows better electrochemical performance, which is probably due to decreased diffusion resistance between 3Co-Ni(OH)<sub>2</sub> ultrafine particles.

**Table 2.** Comparison of electrochemical performances of 3Co-Ni(OH)<sub>2</sub> and other materials

Materials	Current Density (A g <sup>-1</sup> )	Specific Capacitance (F g <sup>-1</sup> )	Cycles Stability	Reference
Ni–Al layered double hydroxide	1	560	80% (1000 cycles)	[28]
Ni-Co hydroxide nanosheets arrays	1	293.3	87.5% (1000 cycles)	[29]
Ni/Al layered double hydroxide	1	482	94% (400 cycles)	[30]
Co-doped Ni(OH) <sub>2</sub> ultrafine particles	1	669.57	94% (500 cycles)	This work

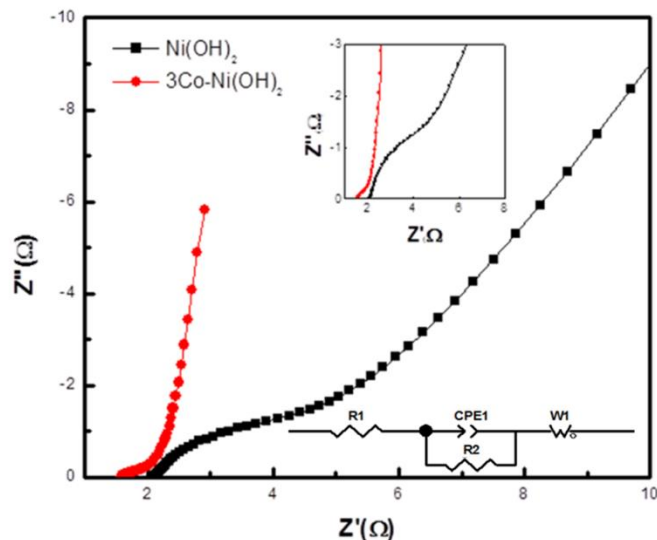


**Figure 7.** Nyquist plots of the  $\text{Ni}(\text{OH})_2$  and  $3\text{Co-Ni}(\text{OH})_2$  electrodes, insets are the details of high frequency and equivalent circuit model

To further elucidate the excellent electrochemical performance of  $3\text{Co-Ni}(\text{OH})_2$  electrode, the electrochemical impedance spectroscopies of  $\text{Ni}(\text{OH})_2$  and  $3\text{Co-Ni}(\text{OH})_2$  materials were studied (shown in Fig.7). The equivalent circuit model (ECM) is also shown in Fig.7. Typically, the Nyquist plot consists of an approximate semicircle at high frequencies and a sloped straight line at low frequencies. In the high frequency region, the  $3\text{Co-Ni}(\text{OH})_2$  electrode shows a smaller intercept on the horizontal axis, indicating that the internal resistance of the  $3\text{Co-Ni}(\text{OH})_2$  electrode is smaller [31]. The diameter of semicircular reflects the charge transfer resistance ( $R_2$ ) caused by the Faraday reaction and the electrochemical double layer capacitance. The  $3\text{Co-Ni}(\text{OH})_2$  electrode has a smaller charge transfer resistance than the  $\text{Ni}(\text{OH})_2$  electrode, corresponding to a high specific capacitance [13].

#### 4. CONCLUSIONS

Co-doped  $\text{Ni}(\text{OH})_2$  ultrafine particles were successfully synthesized by coprecipitation method. The results show that when the molar ratio of  $\text{Ni}^{2+}:\text{Co}^{2+}$  is 5:1,  $\text{Co-Ni}(\text{OH})_2$  material exhibits a high specific capacitance ( $669.57 \text{ F g}^{-1}$ ) at current density  $1 \text{ A g}^{-1}$ , and high cycle stability (94% specific capacitance retention rate after 500 galvanostatic charge-discharge cycles at a high current density of  $16 \text{ A g}^{-1}$ ), showing excellent electrochemical performance. The specific capacitance increase is due to the formation of conductive  $\text{CoOOH}$  in ultrafine particles during the charge process, which can effectively improve the conductivity of  $\text{Ni}(\text{OH})_2$  electrode. Co-doped  $\text{Ni}(\text{OH})_2$  is a promising supercapacitor electrode material.

#### ACKNOWLEDGEMENTS

We gratefully acknowledge National Natural Sciences Foundation of China (Grant No. 21676010) for financial support.

## References

1. G. Wang, L. Zhang and J. Zhang, *Chem. Soc. Rev.*, 41 (2012) 797.
2. M. Inagaki, H. Konno and O. Tanaike, *J. Power Sources*, 195 (2010) 7880.
3. A. González, E. Goikolea, J. A. Barrena and R. Mysyk, *Renew. Sustain. Energy Rev.*, 58 (2016) 1189.
4. Y. Zhang, Y. Gui, X. Wu, H. Feng, A. Zhang, L. Wang and T. Xia, *Int. J. Hydrogen Energy*, 34 (2009) 2467.
5. Z. S. Iro, C. Subramani, and S. S. Dash, *Int. J. Electrochem. Sci.*, 11 (2016) 10628.
6. E. Lim, C. Jo and J. Lee, *Nanoscale*, 8 (2016) 7827.
7. Y. Hsu, Y. Chen, Y. Lin, L. Chen and K. Chen, *Chem. Commun.*, 47 (2011) 1252.
8. Y. Li, Y. Liu, W. Zhang, C. Guo and C. Chen, *Mater. Lett.*, 157 (2015) 273.
9. Y. Wang, Z. Yin, Z. Wang, X. Li, H. Guo, J. Wang and D. Zhang, *Electrochim. Acta*, 293 (2019) 40.
10. Q. Wang, S. Liu, H. Sun and Q. Lu, *RSC Adv.*, 5 (2015) 48181.
11. K. W. Nam, W. S. Yoon and K. B. Kim, *Electrochim. Acta*, 47 (2002) 3201.
12. H. Chen, J. Wang, T. Pan, Y. Zhao, J. Zhang and C. Cao, *J. Electrochem. Soc.*, 150 (2003) A1399.
13. J. Xu, Y. Dong, J. Cao, B. Guo, W. Wang and Z. Chen, *Electrochim. Acta*, 114 (2013) 76.
14. L. Liu, Y. Hou, Y. Gao, N. Yang, J. Li and X. Wang, *Electrochim. Acta*, 295 (2019) 340.
15. N. Jing, A. Zhou, Y. Xiang, and Q. Xu, *Mater. Chem. Phys.*, 205 (2018) 480.
16. J. Yan, Z. Fan, W. Sun, G. Ning, T. Wei, Q. Zhang, R. Zhang, L. Zhi and F. Wei, *Adv. Funct. Mater.*, 22 (2012) 2632.
17. Y. Wang, S. Gai, N. Niu, F. He and P. Yang, *J. Mater. Chem. A*, 1 (2013) 9083.
18. Z. Zhu, Y. Zhou, S. Wang, C. Zhao, Z. Li, G. Chen and C. Zhao, *Electrochim. Acta*, 284 (2018) 444.
19. Z. Wang, P. Hong, S. Peng, T. Zhou, Y. Yang, X. Xing, Z. Wang, R. Zhao, Z. Yan and Y. Wang, *Electrochim. Acta*, 299 (2019) 312.
20. X. Xiong, D. Ding, D. Chen, G. Waller, Y. Bu, Z. Wang and M. Liu, *Nano Energy*, 11 (2015) 154.
21. J. Zhang, L. Kong, J. Cai, Y. Luo and L. Kang, *J. Solid State Electrochem.*, 14 (2010) 2065.
22. L. Xie, Z. Hu, C. Lv, G. Sun, J. Wang, Y. Li, H. He, J. Wang and K. Li, *Electrochim. Acta*, 78 (2012) 205.
23. C. Tanggarnjanavalukul, N. Phattharasupakun, J. Wutthiprom, P. Kidkhunthod and M. Sawangphruk, *Electrochim. Acta*, 273 (2018) 17.
24. L. Zhang, S. Song and H. Shi, *J. Alloys Compd.*, 751 (2018) 69.
25. X. Chen, C. Long, C. Lin, T. Wei, J. Yan, L. Jiang and Z. Fan, *Electrochim. Acta*, 137 (2014) 352.
26. J. Li, M. Yang, J. Wei and Z. Zhou, *Nanoscale*, 4 (2012) 4498.
27. L. Chang, F. Ren, C. Zhao and X. Xue, *J. Electroanal. Chem.*, 778 (2016) 110.
28. B. Wang, Q. Liu, Z. Qian, X. Zhang, J. Wang, Z. Li, H. Yan, Z. Gao, F. Zhao and L. Liu, *J. Power Sources*, 246 (2014) 747.
29. H. Wan, L. Li, Q. Tan, X. Liu, H. Wang and H. Wang, *Nanotech.*, 29 (2018) 194003.
30. J. Wang, Y. Song, Z. Li, Q. Liu, J. Zhou, X. Jing, M. Zhang and Z. Jiang, *Energy Fuels*, 24 (2010) 6463.
31. X. Wang, W. Liu, X. Lu and P. Lee, *J. Mater. Chem.*, 22 (2012) 23114.